Manipulation of intrinsic quantum anomalous Hall effect in two-dimensional $MoYN_2CSCl$ MXene

Yezhu Lv(吕叶竹), Peiji Wang(王培吉), and Changwen Zhang(张昌文)†

School of Physics and Technology, Institute of Spintronics, University of Jinan, Jinan 250022, *China*

(Received 11 June 2022; revised manuscript received 13 August 2022; accepted manuscript online 16 August 2022)

Quantum anomalous Hall effect (QAHE) is an innovative topological spintronic phenomenon with dissipationless chiral edge states and attracts rapidly increasing attention. However, it has only been observed in few materials in experiments. Here, according to the first-principles calculations, we report that the MXene $MoYN_2CSCl$ shows a topologically nontrivial band gap of 37.3 meV, possessing QAHE with a Chern number of $C = 1$, which is induced by band inversion between d_{xz} and d_{yz} orbitals. Also, the topological phase transition for the $MoYN_2CSCl$ can be realized via strain or by turning the magnetization direction. Remarkably, $MoYN_2CSCl$ shows the nodal-line semimetal state dependent on the electron correlation U. Our findings add an experimentally accessible and tunable member to the QAHE family, which stands a chance of enriching the applications in spintronics.

Keywords: $MoYN_2CSCl$ MXene, quantum anomalous Hall effect, topological phase, first-principles calculations

PACS: 73.20.At, 73.43.–f, 73.43.Nq **DOI:** 10.1088/1674-1056/ac89d5

1. Introduction

Research on two-dimensional (2D) materials arises from the exploration of graphene,[1,2] which has different properties from three-dimensional (3D) structures. Following the synthesis of Ti_3C_2, MXenes have aroused extensive attention in the last few years.[3–5] It represents a great family of 2D transition metal (TM) carbides that are chemically exfoliated from the layered MAX phases. The MAX phases host a generic formula of $M_{n+1}AX_n$, in which M refers to an early TM, while A usually corresponds to the group IIIA or IVA element, and X represents C or/and N, with $n = 1$–3.[6,7] MXenes which contain a single TM element, for example, Ti_2C, Nb_2C and Ti_3C_2 have firstly been synthesized in experiments.[3] In these days, a new kind of MXenes containing ordered double TM elements, for example, Mo_2TiC_2 and Cr_2TiC_2, have also been found.[7,8]

MXenes have exhibited an array of physical characters, for instance, metallicity owning excellent conductivity,[5] and half-metallic ferromagnetism.[9] The tantalizing topological properties of MXenes have been demonstrated theoretically. Undoubtedly, MXenes can be one of the best classes of materials for the exploration of the QAHE,[10] and it is possible to tune their spin–orbit coupling (SOC) strength and magnetism by replacing the transition metals or by changing the surfaces,[11] which opens rich possibilities of MXenes in numerous applications.

Different from quantum spin Hall conductivity protected from time reversal symmetry,[12,13] an intriguing quantum phenomenon with topological property, QAHE, appears with intrinsically broken time reversal symmetry, and is generically introduced by the internal magnetism.[14] The QAHE was originally predicted in theory by Haldane,[15] and described by the quantized Hall conductance without magnetic field.[16] Some 2D materials like TM doped topological insulators,[17–19] and TM decorated graphene,[20,21] are reported to harbor the QAHE in theory. Among these materials, a global band gap is generated around the Fermi level due to the adoption of SOC, giving rise to the topologically nontrivial character. In addition, the QAHE insulators are known as Chern insulators as well,[22,23] because of their nonzero topological invariant Chern number.

Owing to its dissipationless chiral edge state, the QAHE can be adopted to engineer next-generation high efficiency electronic devices.[24,25] Until now, diverse methods have been proposed to achieve the QAHE. Two recipes are frequently applied to combine magnetism with TIs, including doping magnetic atoms into TIs[17,26] and building a TI/magnet heterostructure.[27] The former is inclined to render the doped bulk inhomogeneous, leading to the low temperature for observation, which is detrimental to the formation of the QAHE. The latter may suffer from interfacial band bending.[27,28] Therefore, the acquired systems are usually not satisfactory.

Here, according to the first-principles calculations, we present the discovery of the intrinsic QAHE in the 2D $MoYN_2CSCl$ MXene. It is found that the monolayer $MoYN_2CSCl$ is a ferromagnetic QAHE insulator manifesting a direct band gap around 37.3 meV with topologically nontrivial property, hosting a room-temperature estimated to be 619.1 K. We will present structure and stability, electronic structure of the monolayer $MoYN_2CSCl$. The edge states, Berry curvature and the conductivity are considered to affirm

†Corresponding author. E-mail: ss_zhangchw@ujn.edu.cn

© 2022 Chinese Physical Society and IOP Publishing Ltd

that the nontrivial topological characters of the $MoYN_2CSCl$ possessing a Chern number of $C = 1$. We also discuss the band structures and topological phases of the $MoYN_2CSCl$ with respect to changing strains and controlling of magnetic axis direction, as well as different electronic correlation effect. The obtained abundant physical properties make the monolayer $MoYN_2CSCl$ an excellent candidate for prospective applications of the QAHE and spintronics devices.

2. Computational details

The first-principles calculations were carried out by utilizing the projected augmented-wave method as implemented in the Vienna *ab initio* simulation package (VASP).[29,30] The generalized gradient approximation (GGA) in the form of Perdew–Burke–Ernzerhof type was employed to describe the exchange–correlation interaction.[31] The vacuum buffer space larger than 15 Å was applied to prevent the coupling between adjacent slabs. The kinetic energy cutoff of the plane wave was 500 eV. During the structural relaxation, each atom could relax until the Hellmann–Feynman force was smaller than 0.001 eV/Å. A Γ-centered $9\times9\times1$ Monkhorst–Pack k-point grid was utilized to sample the Brillouin zone. Besides, we included the van der Waals (vdW) interactions in all calculations. In consideration of the correlation effects of Y 3d electrons and Mo 3d electrons, we adopted the GGA$+U$ approach with $U = 3$ eV and 2.4 eV for Y and Mo atom, respectively. For the sake of better description on the topological characters, Berry curvature, edge states and anomalous Hall conductivity were also presented by the maximally localized Wannier functions by utilizing WANNIER90 package.[32,33]

3. Results and discussion

The equilibrium lattice constants $a = b = 3.53$ Å of the monolayer $MoYN_2CSCl$ are obtained via energy calculation. The $MoYN_2CSCl$ constitutes by seven atomic layers that stack in the order of S–C–N–Y–N–Mo–Cl, as illustrate in Fig. 1(a), where Y and Mo are transition metals. The local magnetic moment of the Mo atom is $2.089\mu_B$. Thus, Mo atom mainly contributes to the spin polarizations. After the structural relaxation, the atom sites and bond lengths slightly differ from those of the primitive structure. The structural stability is taken into consideration by calculating the phonon spectra, as is illustrated in Fig. 1(b). No negative frequencies are found, indicating the dynamic stability of the $MoYN_2CSCl$.

Then we calculate the binding energies by

$$E_b = E_{MoYN_2CSCl} - E_S - E_C - 2E_N - E_Y - E_{Mo} - E_{Cl}, \quad (1)$$

where E_{MoYN_2CSCl} reprensents the total energy of the monolayer $MoYN_2CSCl$, and other energies like E_S and E_C represent the energies of atom S and C, respectively. The binding energy of the monolayer $MoYN_2CSCl$ has been determined to be $E_b = -30.98$ eV, indicating that the monolayer can stably exist.

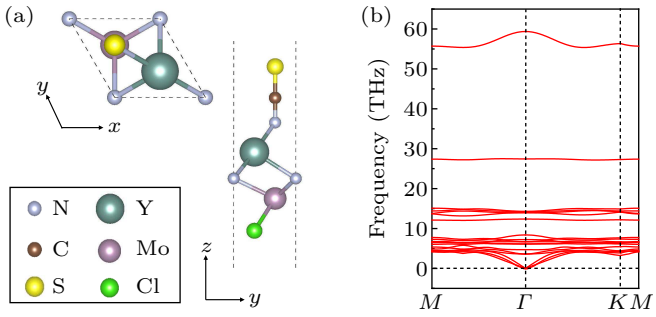


Fig. 1. (a) Top and side views of the atomic structure of the $MoYN_2CSCl$. (b) Phonon spectrum of the $MoYN_2CSCl$.

It is also important to examine the mechanical stability of the monolayer $MoYN_2CSCl$ by calculating elastic constants. In this 2D system, the elastic constants constitute a symmetric 6×6 tensor matrix.[34,35] The calculated results show that C_{11}, C_{12}, C_{22}, and C_{44} are 560.3 N/m, 167.8 N/m, 540.7 N/m, and 194.9 N/m, respectively. The calculated C_{ij} satisfy with the Born criteria of mechanical stability[36] $C_{11}, C_{44} > 0$ and $C_{11}C_{22} - C_{12}^2 > 0$, which confirms the mechanical stability of the $MoYN_2CSCl$. Due to the hexagonal symmetry, the monolayer $MoYN_2CSCl$ is mechanically isotropic. The 2D Youngs moduli C^{2D}, shear modulus G^{2D} and Poisson's ratios v^{2D} can be simply expressed as[37,38]

$$C^{2D} = \frac{C_{11}^2 - C_{12}^2}{C_{11}}, \quad (2)$$

$$G^{2D} = \frac{C_{11} - C_{12}}{2}, \quad (3)$$

$$v^{2D} = \frac{C_{12}}{C_{11}}. \quad (4)$$

The calculated Young's moduli C^{2D}, shear modulus G^{2D} and Poisson's ratio v^{2D} are 510 N/m, 196.3 N/m, and 0.299, respectively. The measured $MoYN_2CSCl$ possesses an ultrahigh stiffness, which is critical to avoid the curling of the 2D material.[39,40]

The magnetic ground state of the monolayer $MoYN_2CSCl$ is determined by comparing the energies of the ferromagnetic (FM) state and the three kinds of antiferromagnetic (AFM) configurations, as plotted in the Fig. 2(a). The results determine that the FM order is the most stable magnetic state. To inspect the spin dynamical stability against temperature, Curie temperature (T_C) is evaluated by utilizing Monte Carlo (MC) simulations, which is in the light of the standard 2D Heisenberg model expressed as

$$H = -J\sum_{i,j} S_i \cdot S_j, \quad (5)$$

where S_i and S_j are spin operator at sites i and j, respectively,

and J is the exchange coupling. Here, we use the variant expression

$$H = -\sum_{i,j} J_{ij} S_i \cdot S_j - A \sum_i (S_i^z)^2, \tag{6}$$

where J_{ij} refers to the exchange coupling constant from i site to j site, and A represents the anisotropy energy parameter. S_i and S_j are the local magnetic moments at i site and j site, while S_i^z means the z component of spin vector. The summation runs over all nearest-neighbor Mo atoms. Taking into account the first nearest site pairs merely, for each magnetic atom, we can obtain

$$E_{\mathrm{FM}} = E_0 - 6J|S|^2 - A|S^z|^2, \tag{7}$$

$$E_{\mathrm{AFM}} = E_0 + 2J|S|^2 - A|S^z|^2. \tag{8}$$

Thus, we can infer

$$J_{\mathrm{unitcell}} = \frac{E_{\mathrm{AFM}} - E_{\mathrm{FM}}}{8|S|^2}. \tag{9}$$

For a $2 \times 2 \times 1$ supercell, there are four magnetic atoms and corresponding to 32 pairs of exchange interaction. However, each magnetic atom in the supercell can be treated as the nearest neighbor twice. Considering the repeated calculation, we obtain

$$J = (E'_{\mathrm{AFM}} - E'_{\mathrm{FM}})/16|S|^2. \tag{10}$$

Here, E'_{AFM} and E'_{FM} signify the total energy of the AFM and FM configurations in the supercell, respectively. Then J is calculated to be 14.63 meV, indicating the FM exchange coupling. At the same time, we calculate the heat capacity (C_{V}) as follows:

$$C_{\mathrm{V}} = \lim_{\Delta T \to 0} \frac{\Delta E_T}{\Delta T}. \tag{11}$$

Here, ΔE_T represents that the alteration of the total energy accompanies the temperature rising from T to $T + \Delta T$. Figure 2(b) shows that T_{C} is estimated to be 619.1 K, which is expected to become a feasible member for spintronic applications with the high-temperature QAHE.

The comprehension of the microscopic origin of FM coupling in the $MoYN_2CSCl$ is that there exists a contest between direct exchange coupling (Mo–Mo) and the superexchange coupling (Mo–X–Mo, X = N or Cl), according to Fig. 3(a). There is a direct coupling between the nearest-neighbor Mo, whose d orbitals have a direct overlap, leading to AFM coupling. It is proposed by the Goodenough–Kanamori–Anderson (GKA) rule[41,42] that the FM coupling is energy favorable with 90° bond angle. Based on the Heitler–London model,[43] the approximate form of $J \approx 2k + 4\beta S$ is reported, where J refers to the exchange integral in a 2D material. And the first term k is known as a potential exchange that is positive according to the Hund's first rule.[44] The second term composes of the hopping integral β and overlap integral S. On account of the bond angles of Mo–N–Mo (102.14°) and Mo–Cl–Mo (85.50°) closed to 90°, the Mo-d orbitals seem to be approximately orthogonal to the p orbitals of N and Cl, giving rise to an inappreciable overlap integral, then consequently a positive $J \approx 2k$. As a result, the 2D monolayer $MoYN_2CSCl$ possesses an ordering of ferromagnetism according to the comparatively large FM superexchange interaction.

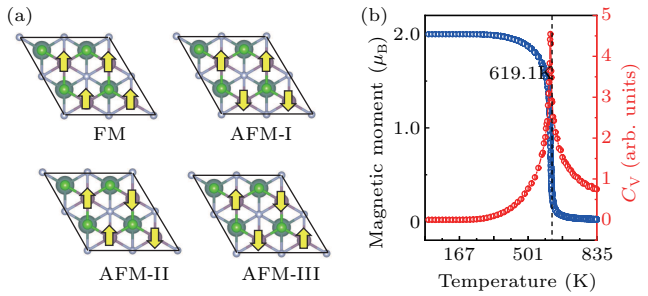


Fig. 2. (a) Four magnetic configurations (FM and AFM-I, AFM-II, AFM-III). The arrows indicate the orientations of magnetic moment. (b) The simulated magnetic moment and specific heat (C_{V}) as functions of temperature.

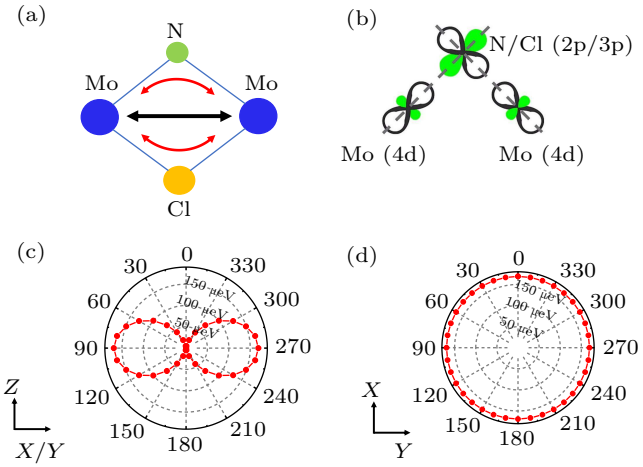


Fig. 3. (a) Schematic diagrams of direct exchange Mo–Mo (black arrows) and superexchange Mo–N(Cl)–Mo (red arrows) interactions. (b) Mechanism of superexchange interaction for the Mo–N(Cl)–Mo bond angle. (c) and (d) Variation of the MAE for the pristine $MoYN_2CSCl$ on the polar angle θ and azimuth angle φ, respectively.

Besides, magnetic anisotropy energy (MAE) denotes the energy required to change the magnetic moment orientation from the easy axis to the hard axis. The MAE, regulated by $\mathrm{MAE}(\theta,\varphi) = E(\theta,\varphi) - E(\theta = 0°, \varphi = 0°)$ [$E(\theta,\varphi)$ refers to the total energy when the spin magnetic moment S points to the polar angle θ and azimuthal angle φ], is computed by rotating the spin magnetic moment along the xy and xz/yz planes, as can be seen in Figs. 3(c) and 3(d). We observe that the MAE strongly depends on θ, and hardly depends on φ. MAE is calculated to be 0 at $\theta = 0°$ or 180° , and attains a maximum value around 169 μeV within the xy plane, manifesting that the monolayer $MoYN_2CSCl$ is along out of the plane direction. The long-range order can be damaged if the heat fluctuation exists, but the large MAE obtained here is in favor of stabilizing this ordering at a relatively high temperature.

To get an in-depth understanding on electronic characters of the FM $MoYN_2CSCl$ MXene, we investigate the band structure in detail. Both GGA + U and GGA + U + SOC band structures of the $MoYN_2CSCl$ are illustrated in Figs. 4(a) and 4(b), as well as the corresponding partial band projections. The electronic structures of the spin-up and spin-down electronic orbits reveal distinct conducting behaviors. The monolayer $MoYN_2CSCl$ is a half-metal which offers 100% spin polarization intrinsically around the Fermi level. The spin-up bands show a wide band gap, manifesting the insulating character, while the other channel possesses metallic conduction. According to the C_3 symmetry, the d orbitals of the Mo atom enclosed by the octahedral with distortion are divided into three parts d_{z^2}, $(d_{xy}, d_{x^2-y^2})$, and (d_{xz}, d_{yz}). Without SOC, the system is gapless with the degenerated Mo-d_{xz}/d_{yz} orbitals around the Γ point between the valence and conduction bands. Additionally, we can see that the valence band at the K point is mainly contributed by Mo-d_{z^2}, as displayed in Fig. 4(c). The degeneracy of d_{xz} and d_{yz} orbitals at Γ point is protected by C_3 symmetry. When considering the effect of SOC, C_3 symmetry is broken, thus the doubly degenerate Mo-d_{xz}/d_{yz} orbitals split into two parts, leading to an energy gap with band inversion between them. Prominently, the E_F in Fig. 4(d) is within the SOC-induced band gap. The SOC induced band inversion is identified as the common mechanism of TIs. It is the heavy atom Mo in the $MoYN_2CSCl$ produces the strong SOC and results in an inverted energy gap. The energy gap of the $MoYN_2CSCl$ reaches 37.3 meV, which is crucial for the realization of the QAHE.

To testify their topological nature, the chiral edge state of the $MoYN_2CSCl$ is exhibited in Fig. 5(a). We can clearly observe one metallic edge state existing along the $\Gamma \to M$ path, corresponding to the QAHE insulators. The QAH conductance σ_{xy} can also be obtained in the light of Chern number C as[45]

$$\sigma_{xy} = \frac{e^2}{2\pi h}\int \mathrm{d}k_x \mathrm{d}k_y b_z(k) = \frac{e^2}{h}C, \tag{12}$$

where $b_z(k)$ refers to the z component of the Berry curvature

$$b_z(k) = -\mathrm{Im}\langle \partial_k u(k)| \times |\partial_k u(k)\rangle, \tag{13}$$

and $u(k)$ represents the periodic part of the Bloch function.

Within the energy gap range, the value of σ_{xy} is exactly quantized to e^2/h, and consistent with $C = 1$, as plotted in Fig. 5(b). At the same time, figure 5(c) indicates that a nonzero Berry curvature appears around the Γ point, which agrees with the calculated chiral edge states.

Applying diverse strain may have an impact on the electronic structures of materials. Figure 6 exhibits the energy gaps of the FM monolayer $MoYN_2CSCl$ at different strains. The isotropic strain is defined as

$$\varepsilon = 100 \times (a - a_0)\,\%, \tag{14}$$

where a and a_0 denote the lattice constants of the strained and unstrained, respectively. Depending on Eq. (14), a negative ε represents the strain with compression, and a positive ε indicates the strain with tension.

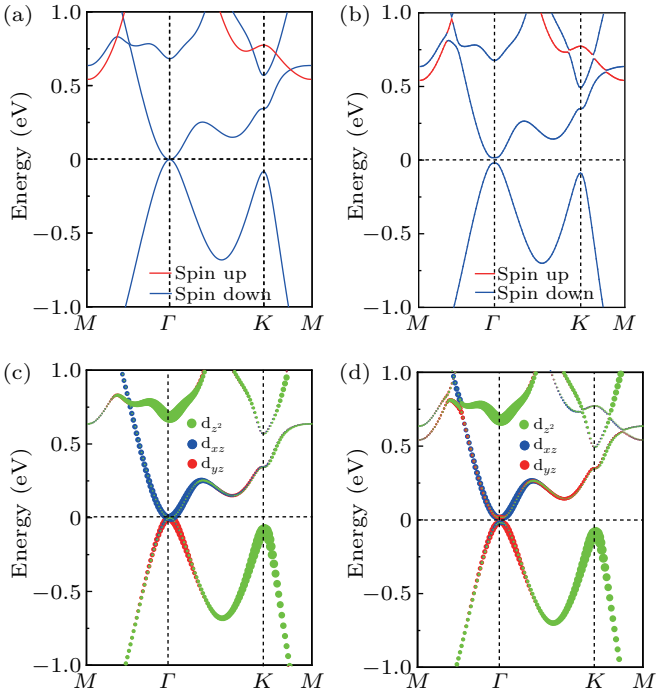


Fig. 4. Band structure of the $MoYN_2CSCl$ with $U = 2.40$ eV (a) DFT + U and (b) DFT + U + SOC. (c) and (d) The partial band projections of (a) and (b), respectively.

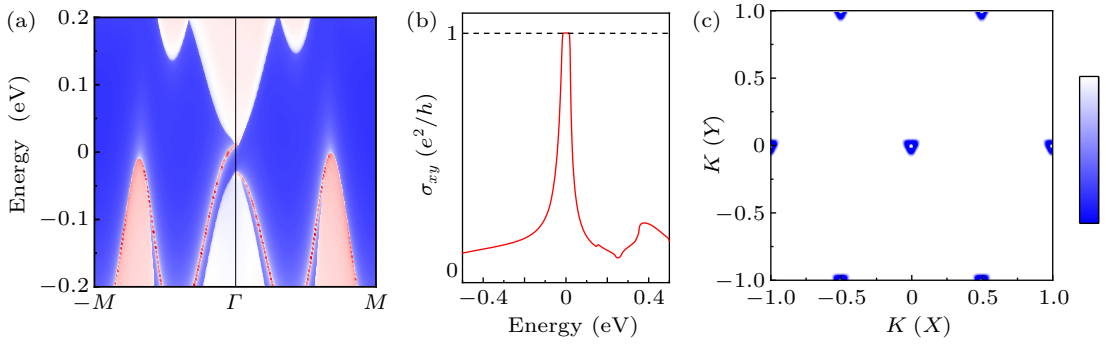


Fig. 5. (a) The chiral edge state of the $MoYN_2CSCl$. (b) Calculated Anomalous Hall conductance of the $MoYN_2CSCl$. (c) Berry curvature distribution within the first Brillouin zone.

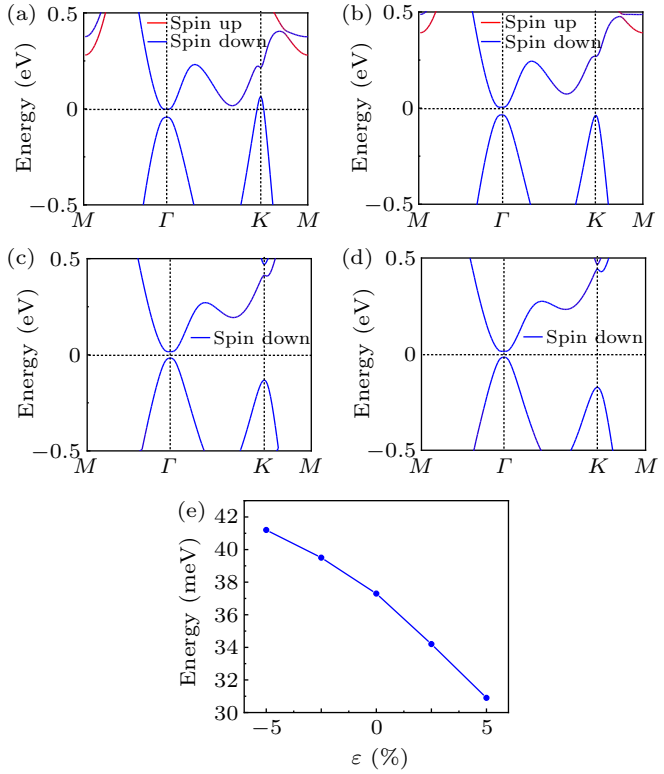


Fig. 6. Band structures of the monolayer $MoYN_2CSCl$ in the presence of SOC in $\varepsilon = -5\%$ (a), $\varepsilon = -2.5\%$ (b), $\varepsilon = 2.5\%$ (c), $\varepsilon = 5\%$ (d). (e) Monolayer energy gap as a function of biaxial in-plane strain.

For a monolayer $MoYN_2CSCl$, the threefold rotation symmetry preserves with the varying biaxial strain. In the absence of SOC, the degenerate point near the Γ point is insensitive with strain. In the presence of SOC, the bands around the Fermi level are really sensitive to applied strains, as plotted in Fig. 6. The energy gap decreases monotonously as the strain changes from $\varepsilon = -5\%$ to $\varepsilon = 5\%$. In this case, the valence band energy at the K point decreases significantly.

However, the character of band inversion at Γ point preserves. When applying the tensile strain, as ε varies from 0 to 5.0%, the monolayer structure possesses the robust QAHE. However, under small compressive strains, the nontrivial band topology vanishes at $\varepsilon = -5\%$, due to the gapless state between the bottom of conduction band and the top of valence band.

Besides, we consider the effect of magnetic orientation on the topological property. When the magnetic axis is in the z-direction, the monolayer $MoYN_2CSCl$ shows a Chern-number ($C = 1$) phase. By turning the magnetization to x-direction, it reveals that the nontrivial topological property disappears, and the trivial topological property of the $MoYN_2CSCl$ originates from no band inversion between the d_{xz} and d_{yz} bands.

In this work, the electronic correlation[46–48] on band structures of the monolayer $MoYN_2CSCl$ are considered comprehensively by the GGA$+U+$SOC approach. The GGA$+U$ calculation indicates their exchange energies are in connection with the effective U values. Diverse U ranging from 0 eV to 3 eV are used for the Mo atom. Upon further increasing U, we find that without SOC the degenerate parts are getting close to the Fermi level, as plotted in Figs. 7(a), 7(c), and 7(e). When electronic structures of the $MoYN_2CSCl$ monolayer with SOC are calculated, the degenerate part at Γ point turns to an energy gap, whose size is in direct proportion to the U value. As we can see in Fig. 7(f), the gap reaches 43.1 meV when $U = 3$ eV.

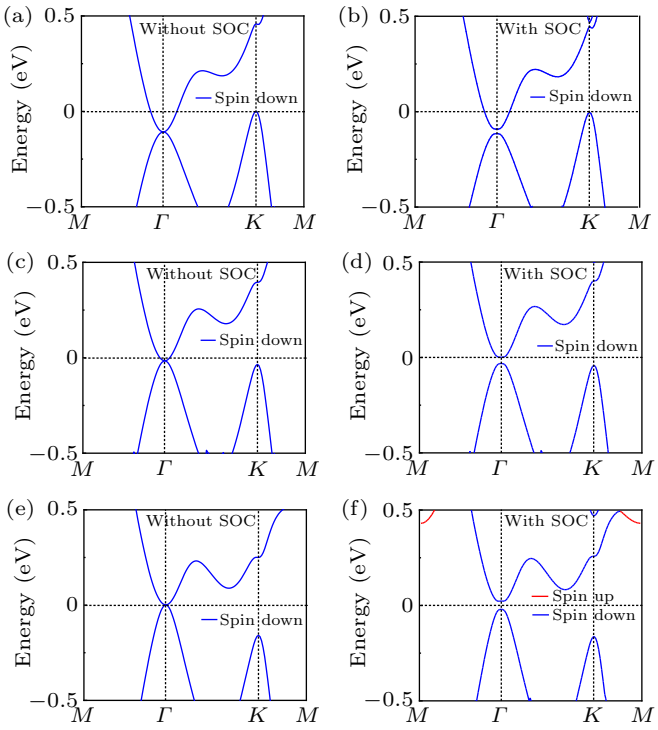


Fig. 7. Band structures of the monolayer $MoYN_2CSCl$ in the absence of SOC in $U = 1$ eV (a), $U = 2$ eV (c), $U = 3$ eV (e). (b), (d) and (f) Bands with SOC corresponding to (a), (c), and (e), respectively.

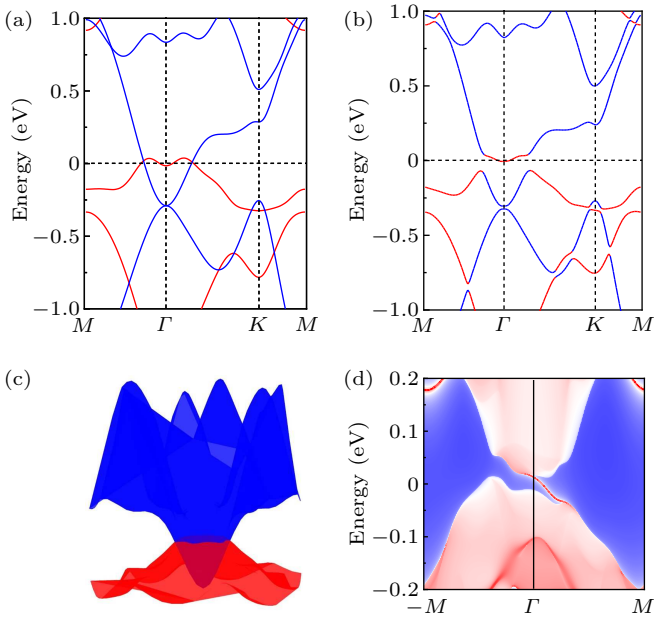


Fig. 8. (a) and (b) Electronic structures of the monolayer $MoYN_2CSCl$ without and with SOC in $U = 0$ eV. Red and blue curves denote spin-up and spin-down channels, respectively. (c) The corresponding three-dimensional view of the $MoYN_2CSCl$. (d) The chiral edge state of the $MoYN_2CSCl$ in $U = 0$ eV.

While there is a difference in $U = 0$ eV, without considering SOC, the electronic structure of the monolayer $MoYN_2CSCl$ is investigated, as illustrated in Fig. 8(a). Near the Fermi level, there are two inverted bands possessing opposite spins crossing, demonstrating the appearance of a 2D nodal-line semimetal.[49–53] While turning on SOC, figure 8(b) shows that a SOC band gap ($\sim$ 111 meV) is produced along the nodal line and leads to the QAHE with $C = 1$. One can observe that an edge state with nontrivial topological property appears inside the SOC-induced gap.

4. Conclusion and perspectives

According to the first-principles DFT calculations, we systematically investigate a 2D $MoYN_2CSCl$ monolayer, which is an intrinsic FM QAHE insulator with Curie temperature estimated to be 619.1 K. Significantly, the SOC induces a topologically nontrivial band gap of 37.3 meV possessing a Chern number $C = 1$ induced by band inversion between d_{xz} and d_{yz} orbitals. Additionally, we research the manipulation of nontrivial band gap by utilizing strain and regulating magnetic axis from the z-direction to x-direction, which leads to a vanishing of nontrivial topological property. Including different Hubbard U, we find that when $U = 0$ eV the $MoYN_2CSCl$ transforms to a nodal-line semimetal with Chern number $C = 1$. Furthermore, providing guidelines for future discovery and design, we expect experimental verifications of the QAHE in the monolayer $MoYN_2CSCl$.

Acknowledgments

Project supported by Taishan Scholar Program of Shandong Province, China (Grant No. ts20190939), Independent Cultivation Program of Innovation Team of Jinan City (Grant No. 2021GXRC043), Shandong Provincial Natural Science Foundation (Grant No. ZR2020QA052), and National Natural Science Foundation of China (Grant Nos. 52173283 and 62071200).

References

[1] Hwang E H, Rossi E and Sarma S D 2009 *Phys. Rev. B* **80** 235415
[2] Sun H, Li S S, Ji W X and Zhang C W 2022 *Phys. Rev. B* **105** 195112
[3] Naguib M, Kurtoglu M, Presser V, Lu J, Niu J, Heon M, Hultman L, Gogotsi Y and Barsoum M W 2011 *Adv. Mater.* **23** 4248
[4] Naguib M, Mochalin V N, Barsoum M W and Gogotsi Y 2014 *Adv. Mater.* **26** 992
[5] Feng X, He Z, Peng R, Dai Y, Huang B and Ma Y 2022 *Phys. Rev. Mater.* **6** 044001
[6] Naguib M, Mashtalir O, Carle J, Presser V, Lu J, Hultman L, Gogotsi Y and Barsoum M W 2012 *ACS Nano* **6** 1322
[7] Si C, Jin K H, Zhou J, Sun Z and Liu F 2016 *Nano Lett.* **16** 6584
[8] Anasori B, Xie Y, Beidaghi M, Lu J, Hosler B C, Hultman L, Kent P R C, Gogotsi Y and Barsoum M W 2015 *ACS Nano* **9** 9507
[9] Si C, Zhou J and Sun Z 2015 *ACS Appl. Mater. Inter.* **7** 17510
[10] Barik R K and Singh A K 2021 *Chem. Mater.* **33** 6311
[11] Khazaei M, Ranjbar A, Arai M, Sasaki T and Yunoki S 2017 *J. Mater. Chem. C* **5** 2488
[12] Kane C L and Mele E J 2005 *Phys. Rev. Lett.* **95** 226801
[13] Zhang S B, Zhang Y Y and Shen S Q 2014 *Phys. Rev. B* **90** 115305
[14] Huang C, Zhou J, Wu H, Deng K, Jena P and Kan E 2017 *Phys. Rev. B* **95** 045113
[15] Haldane F D M 1988 *Phys. Rev. Lett.* **61** 2015
[16] Gao R, Qin G, Qi S, Qiao Z and Ren W 2021 *Phys. Rev. Mater.* **5** 114201
[17] Yu R, Zhang W, Zhang H J, Zhang S C, Dai X and Fang Z 2010 *Science* **329** 61
[18] Wang Y P, Ji W X, Zhang C W, Li P, Zhang S F, Wang P J, Li S S and Yan S S 2017 *Appl. Phys. Lett.* **110** 213101
[19] Qi S, Qiao Z, Deng X, Cubuk E D, Chen H, Zhu W, Kaxiras E, Zhang S B, Xu X and Zhang Z 2016 *Phys. Rev. Lett.* **117** 056804
[20] Zhang H, Lazo C, Blügel S, Heinze S and Mokrousov Y 2012 *Phys. Rev. Lett.* **108** 056802
[21] Li S S, Ji W X, Hu S J, Zhang C W and Yan S S 2017 *ACS Appl. Mater. Inter.* **9** 41443
[22] Jiang H, Qiao Z, Liu H and Niu Q 2012 *Phys. Rev. B* **85** 45445
[23] Zhang S J, Zhang C W, Zhang S F, Ji W X, Li P, Wang P J, Li S S and Yan S S 2017 *Phys. Rev. B* **96** 205433
[24] He K, Wang Y and Xue Q K 2014 *Natl. Sci. Rev.* **1** 38
[25] Ren Y, Qiao Z and Niu Q 2016 *Rep. Prog. Phys.* **79** 66501
[26] Zhang M H, Zhang C W, Wang P J and Li S S 2018 *Nanoscale* **10** 20226
[27] Luo W and Qi X L 2013 *Phys. Rev. B* **87** 085431
[28] Li P, Yu J, Wang Y and Luo W 2021 *Phys. Rev. B* **103** 155118
[29] Kresse G and Furthmüller J 1996 *Phys. Rev. B* **54** 11169
[30] Mortensen J J, Hansen L B and Jacobsen K W 2005 *Phys. Rev. B* **71** 035109
[31] Shi J M, Peeters F M, Hai G Q and Devreese J T 1992 *Phys. Rev. B* **44** 5692
[32] Mostofi A A, Yates J R, Lee Y S, Souza I, Vanderbilt D and Marzari N 2008 *Comput. Phys. Commun.* **178** 685
[33] Sancho M P L, Sancho J M L and Rubio J 1985 *J. Phys. F: Met. Phys.* **15** 851
[34] Sheng K, Chen Q, Yuan H K and Wang Z Y 2022 *Phys. Rev. B* **105** 075304
[35] Cadelano E, Palla P L, Giordano S and Colombo L 2010 *Phys. Rev. B* **82** 235414
[36] Wu Z J, Zhao E J, Xiang H P, Hao X F, Liu X J and Meng J 2007 *Phys. Rev. B* **76** 054115
[37] Guo S D, Zhu J X, Mu W Q and Liu B G 2021 *Phys. Rev. B* **104** 224428
[38] Cadelano E and Colombo L 2012 *Phys. Rev. B* **85** 245434
[39] Guo G C, Wang R Z, Ming B M, Wang C, Luo S W, Zhang M and Yan H 2019 *J. Mater. Chem. A* **7** 2106
[40] Chitara B and Ya'akobovitz A 2018 *Nanoscale* **10** 13022
[41] Goodenough J B 1955 *Phys. Rev.* **100** 564
[42] Kanamori J 1959 *J. Phys. Chem. Solids* **10** 87
[43] Heitler W and London F 1927 *Z. Phys.* **44** 455
[44] Bonchev D 1981 *Int. J. Quantum Chem.* **19** 673
[45] Šmejkal L, Mokrousov Y, Yan B and MacDonald A H 2018 *Nat. Phys.* **14** 242
[46] Rohringer G, Valli A and Toschi A 2012 *Phys. Rev. B* **86** 125114
[47] Mori H, Tanaka S and Mori T 1998 *Phys. Rev. B* **57** 12023
[48] Fanfarillo L and Bascones E 2015 *Phys. Rev. B* **92** 075136
[49] Jin Y J, Wang R, Zhao J Z, Du Y P, C. Di Zheng, Gan L Y, Liu J F, Xu H and Tong S Y 2017 *Nanoscale* **9** 13112
[50] Liu Z, Zhao G, Liu B, Wang Z F, Yang J and Liu F 2018 *Phys. Rev. Lett.* **121** 246401
[51] Bian G, Chang T R, Zheng H, Velury S, Xu S Y, Neupert T, Chiu C K, Huang S M, Sanchez D S, Belopolski I, Alidoust N, Chen P J, Chang G, Bansil A, Jeng H T, Lin H and Hasan M Z 2016 *Phys. Rev. B* **93** 121113
[52] Xu Q, Yu R, Fang Z, Dai X and Weng H 2017 *Phys. Rev. B* **95** 045136
[53] Shao D F, Gurung G, Zhang S H and Tsymbal E Y 2019 *Phys. Rev. Lett.* **122** 77203